Morphology, Mechanical Properties, and Failure Topography of Semi-Interpenetrating Polymer Networks Based on Natural Rubber and Polystyrene

AJI P. MATHEW,[1] S. PACKIRISAMY,[2] SABU THOMAS[1]

[1] School of Chemical Sciences, Mahatma Gandhi University, Kottayam-686 560, Kerala, India

[2] Polymers and Special Chemicals Division, Vikram Sarabai Space Centre, Thiruvananthapuram-695022, Kerala, India

Received 7 August 1999; accepted 29 March 2000

ABSTRACT: Semi-interpenetrating networks (semi-IPNs) were prepared from natural rubber (NR) and polystyrene (PS) by the sequential method. In these semi-IPNs the NR phase was crosslinked while the PS phase was uncrosslinked. Different initiating systems such as dicumyl peroxide (DCP), benzoyl peroxide (BPO), and the azobisisobutyronitrile (AIBN) system were used for polymerizing the PS phase. The blend ratio was varied by controlling the swelling of NR in the styrene monomer. The mechanical properties of the semi-IPNs, namely, density, tensile strength, tear strength, elongation at break, tension set, tensile set, impact strength, and hardness, were determined. The morphology of different IPNs was studied using scanning electron microscopy. A compact morphology with a homogeneous phase distribution was observed in the semi-IPNs. The properties of the semi-IPN do not change much with the initiating system. However, in most cases, the DCP initiating system showed slightly superior performance. The tensile and tear-strength values of the IPNs were found to increase with increasing plastomer content. The crosslink density of the semi-IPNs also increased with increase in the polystyrene content. The experimental values were compared with theoretical models such as series, parallel, Halpin Tsai, Coran, Takayanaki, Kerner, and Kunori. The tensile and tear-fracture surfaces were examined using a scanning electron microscope. The fracture patterns were correlated with the strength and nature of the failure. © 2000 John Wiley & Sons, Inc. J Appl Polym Sci 78: 2327–2344, 2000

Key words: natural rubber; polystyrene; interpenetrating networks; morphology; mechanical properties

INTRODUCTION

Interpenetrating polymer networks (IPNs) are a novel class of polymer blends in which one or both phases are crosslinked with total or partial physical interlocking.[1–3] IPNs can be defined as a polymer blend in which at least one of the components is polymerized and/or crosslinked in the immediate presence of the other.[4–6] IPNs can be prepared by simultaneous polymerization, sequential polymerization, or latex blending techniques.

These polymer systems display a wide spectrum of properties ranging from toughened elastomers to high-impact plastics.[7,8] The physical nature of the component polymers, their blend ratio, crosslink density, etc., control the ultimate properties of the resulting IPN.[9,10] During IPN formation, intermixing of phases occurs through

Correspondence to: S. Thomas.

Contract grant sponsor: Third World Academy of Sciences (TWAS, Italy).

Journal of Applied Polymer Science, Vol. 78, 2327–2344 (2000)

physical interlocking and thereby the phase separation is limited to some extent. When the two networks are formed simultaneously, the degree of phase separation is small, while in the sequential technique, the ultimate properties depend more on the continuous phase.[11,12]

Although true IPNs are homogeneous mixture of two polymers with no covalent bond existing between network I and network II, in most cases, some degree of graft copolymerization is unavoidable. An interesting range of properties could be attained when an elastomer and plastomer are blended in different proportions for the preparation of an IPN.[13,14] In the case of full IPNs, both phases are crosslinked and two interlocked networks will result. In the case of semi-IPNs, only one of the phases is crosslinked and the other phase is linear. When polymer I alone is crosslinked, the system is named semi-IPN-I. If polymer I is linear and polymer II is crosslinked, it is semi-IPN-II.[15–17] Aspects of phase continuity, molecular mixing at phase boundaries, etc., contribute to the mechanical behavior of these polymer systems. In semi-IPNs, usually the crosslinked phase tends to be the continuous phase.[18,19]

IPN synthesis is highly significant and interesting because it is the only way of blending two crosslinked polymers intimately. Also, a wide range of properties can be obtained depending on the phase morphology.[20–22]

A certain degree of compatibility is introduced between polymers by IPN formation, as the two polymers are interlocked in a three-dimensional network structure during synthesis. Even in systems having low compatibility, the phase domains are smaller than in the case of mechanical blending.[23,24]

The properties of the system developed from a rubber and a plastic are determined by (1) the material properties of the rubber and plastic phase, (2) the rubber/plastic blend ratio, (3) the phase morphology developed, and (4) the molecular mixing at phase boundaries.[25] Yenwo et al. studied the variation of domain size with composition and crosslink density for castor oil–urethane/polystyrene (PS) polymer networks.[4,26] In this system, an increase in the PS concentration decreases the phase domain size, because the domain size of polymer II is quantitatively controlled by the crosslinking of polymer I. In SBR/PS networks developed by Donatelli et al., it was found that if polymer I alone is crosslinked polymer I forms the continuous phase and polymer II becomes phase-continuous or phase-separated depending on the blend ratio.[10–12]

Table I Specifications for ISNR—5-grade NR

Dirt content (% by mass, max)	0.03
Volatile matter (% by mass, max)	0.70
Nitrogen content (% by mass, max)	0.40
Ash content (% by mass, max)	0.48
Initial plasticity ($P0$, min)	40.0
Plasticity retention index (PRI, min)	75.0
Intrinsic viscosity [η] (dL/g)	4.45×10^5

In the present study, semi-IPNs were synthesized from natural rubber, and the styrene monomer, by the sequential technique. Natural rubber (NR) has excellent elastic properties and good damping characteristics. PS is a transparent brittle thermoplastic with poor weathering properties. It has a low heat-distortion temperature (85°C) and outdoor exposure causes yellowing and crazing of the polymer. The impact properties of PS can be enhanced by blending it with NR. The blending could be made more effective by IPN synthesis. Through IPN preparation, NR and PS phases could be blended in the crosslinked form. The resulting IPN will combine the properties of the component polymers. A wide range of properties could be obtained based on the blend ratio[27–29] and the extent of crosslinking.

In this article, the morphology and the mechanical properties of NR/PS semi-IPNs in which the NR phase was crosslinked and PS was linear were investigated. Attempts were made to correlate the blend morphology with mechanical properties. The influence of the blend composition and crosslink density on the mechanical properties was studied in detail. The effects of various initiating systems on IPN properties were also looked into. Finally, the failure behavior of the IPNs were analyzed by scanning electron microscopy (SEM).

EXPERIMENTAL

Materials Used

NR

The NR used was of Indian standard NR (ISNR-5) grade. It was supplied by the Rubber Research Institute India (RRII) (Kottayam Kerala, India). The specifications of NR are given in Table I.

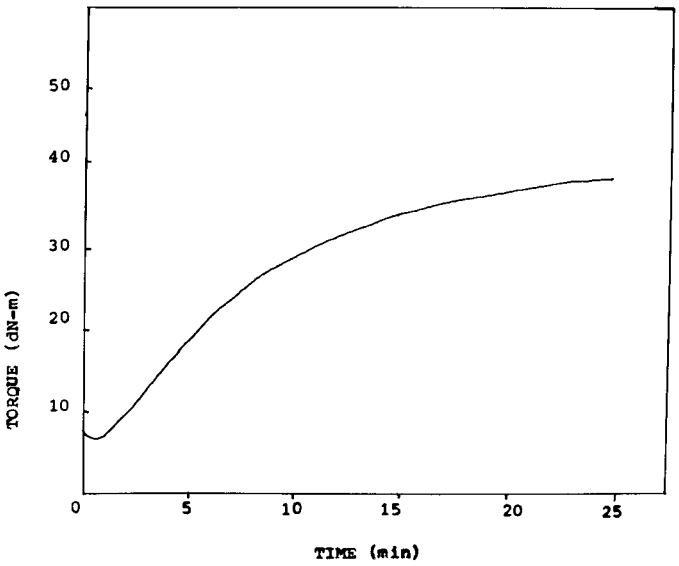

Figure 1 Rheograph of the mix.

Styrene Monomer

The styrene monomer for IPN synthesis was supplied by Merck (India). The monomer was made inhibitor free by washing it with 1% NaOH and it was dried before use.

Initiators

Dicumyl peroxide (DCP) (40% active) was used as the vulcanizing agent for rubber and as the initiator for the polymerization of styrene. It was supplied by Kishore Rubber Products Pvt. Ltd. (Pune, India). Benzoyl peroxide (BPO) was obtained from BDH (Mumbai, India) and was used as the initiator for styrene. Azobisisobutyronitrile (AIBN) was obtained from Sigma (Mumbai, India) and was used as the initiator. Cumene hydroperoxide (CHP) and tetraethylenepentamine (TEP) constitute the redox initiating system. A 10% solution of TEP in water was prepared. Five percent of this solution and 0.5% of CHP (both by volume of styrene) together act as the redox initiator.

IPN Preparation

NR was masticated in a two-roll mixing mill at room temperature. DCP (4 phr) was added and mixed well. The rheograph of the mix was taken on a Monsanto rheometer and the optimum cure time was determined (Fig. 1). The curing characteristics of NR are given in Table II. The mix was cured at 160°C on a hydraulic press to get a crosslinked sheet. The schematic representation of the crosslink formed in a DCP-cured sample is given in Figure 2.

The following different series of IPNs were prepared using different initiators:

Series 1

The crosslinked NR sheets were weighed and kept immersed in an inhibitor-free styrene monomer containing 1% BPO as an initiator. The NR sheets were swollen at different time intervals to obtain different weight percentages of PS. The kinetics of diffusion of styrene through NR were reported by us earlier.[30] The swollen samples were kept at 0°C for a few hours to achieve equilibrium distribution of the styrene monomer in the matrix. The swollen networks were heated at 80°C for 6 h and at 100°C for 2 h in an atmosphre of styrene to complete the polymerization of the styrene monomer. The hardened sheets were then

Table II Formulation and Cure Characteristics of NR Mix

Formulation of the Mixes (phr)		Cure Characteristics	
NR	100	Min torque (dNm)	7
DCP	4	Max torque (dNm)	44.8
		Scorch time (min)	1.8
		Optimum cure (min)	25

phr, parts per hundred rubber.

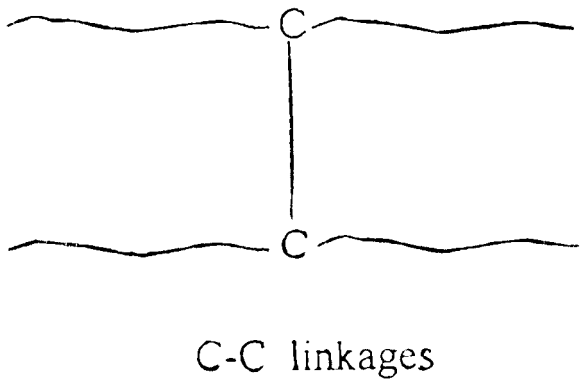

Figure 2 Schematic representation of C—C crosslinks in DCP-cured system.

kept in a vacuum air oven to make it free of unreacted styrene. The final weight of the IPN was taken and the composition of the sample was determined.

Series 2

The redox initiator system consisting of a 10% solution of TEP and 0.5% of CHP was added to the styrene monomer and NR sheets were swollen in it. The swollen samples were polymerized by heating them to a temperature of 80°C for 6 h and at 100°C for 2 h in an atmosphere of styrene.

Series 3

In this method, 1% DCP was added to the styrene monomer and vulcanized NR samples were allowed to swell in it. The swollen sheets were heated at 80°C for 6 h and at 100°C for 2 h in an atmosphere of styrene.

Series 4

In this method, 0.5% AIBN was added to the monomer and the rubber samples were swollen in it. The swollen sheets were polymerized at 80°C for 6 h and at 100°C for 2 hrs in an atmosphere of styrene.

The hardened sheets, in all cases, were kept in a vacuum oven to make it free from unreacted styrene. The final weight of the sample was taken and the composition of the sample was determined. In all four series, NR/PS semi-IPNS with PS content up to 70% were prepared. The semi-IPNs developed using the four initiating systems were named based on the weight percent of NR in each sample. The nomenclature of IPNs are explained in Table III. The codes S_1, S_2, S_3, and S_4 represent series 1, 2, 3, and 4, respectively, as mentioned earlier. The codes N_0, N_{30}, N_{50}, N_{70}, and N_{100} stand for 0, 30, 50, 70, and 100 parts by weight of NR in the blend. Based on the initiating system and the blend ratio, the IPNs are coded.

Measurements

Tensile Properties

Tensile strength (TS) and elongation at break (EB %) were measured using a tensile testing machine at a crosshead speed of 50 mm/min. The TS mea-

Table III Nomenclature of IPNs and Crosslinking Density

Code	Initiator for PS	Weight Fraction		Crosslink Density ($\nu \times 10^4$)	
		NR %	PS %	Tensile Method (gmol/cc)	Swelling Method (gmol/cc)
N_{100}		100	0	0.45	0.94
S_1N_{70}	BPO	70	30	1.38	3.24
S_1N_{50}	BPO	50	50	2.84	5.55
S_1N_{30}	BPO	30	70	4.39	7.06
S_2N_{70}	(CHP & TEP)	70	30	2.06	3.5
S_2N_{50}	(CHP & TEP)	50	50	3.13	4.92
S_2N_{40}	(CHP & TEP)	40	60	9.44	6.24
S_3N_{70}	DCP	70	30	1.57	4.45
S_3N_{50}	DCP	50	50	8.80	6.07
S_3N_{30}	DCP	30	20	15.25	7.43
S_4N_{70}	AIBN	70	30	1.63	3.68
S_4N_{50}	AIBN	50	50	3.23	5.81
S_4N_{30}	AIBN	30	70	5.80	6.98
N_0	—	0	100	—	—

surements were done using dumpbell specimens, at room temperature, as per the ASTM D-80 test method.

Tear Strength

The measurements were done as per ASTM D-624 at a crosshead speed of 50 mm/min.

Tension Set at 100% Elongation

The tension-set values were determined according to ASTM D-412. The samples were kept under tension for a fixed elongation (100%) and time interval, then released from the clamp, kept aside for another fixed time interval, and the change in dimensions determined.

Tensile Set After Failure

The tensile-set values were determined according to ASTM D-412.

Impact Strength

The impact measurements were made on an Impats-15 resilience test pendulum as per the ASTM procedure. Izod impact testings were done after notching the samples and the impact energy and the resilience were obtained. The impact strength measurements were done only for samples with a PS content of 50% and above.

Hardness

The Shore A hardness was measured using a Durometer for the semi-IPNs.

Density

The density of the samples were measured at room temperature using the hydrostatic technique, according to ASTM D-792.

Crosslink Density

The crosslink density of the samples was determined from the TS measurements using the equation

$$\nu = \frac{F}{2A_0RT\rho(\alpha - 1/\alpha^2)} \tag{1}$$

where F is the maximum load; A_0, the area of cross section of the tensile specimen; ρ, the density; R, the universal gas constant; T, the absolute temperature; and α, the extension ratio.[31,32] The crosslink density was determined by swelling method also, using the equation

$$\nu = 1/2Mc \tag{2}$$

where Mc is the molecular weight between crosslinks[33–35]:

$$Mc = \frac{-\rho_p V_r \phi^{1/3}}{[\ln(1 - \phi) + \phi + \chi\phi^2]} \tag{3}$$

where V_r is the molar volume of the solvent; ρ_p, the density of the polymer; χ, the interaction parameter; and ϕ, the volume fraction of the swollen sample. χ is given by

$$\chi = 0.34 + Vr/RT(\delta_A - \delta_B)^2 \tag{4}$$

where δ_A and δ_B are the solubility parameters of the solvent and polymer, respectively; R, the gas constant; and T, the absolute temperature.

The swelling of the IPNs was carried out in toluene and the crosslink density was determined from the swelling method. However, it was found that the crosslink density values obtained by the two different methods show wide variation. This observation was reported by other researchers earlier.

Scanning Electron Microscopy

The phase morphology of cryogenically fractured IPN specimens was examined using a Philips-500 Model scanning electron microscope. Also, the micrographs of the failure surfaces of the tear and tensile specimens were also taken.

RESULTS AND DISCUSSION

The crosslink density of the samples was determined by the swelling method and from the tensile measurement. The crosslink density values are given in Table III. It was found that the crosslink density, in general, increases as we move from N_{70} to N_{30} samples in each series. In all cases, the crosslinks in the NR phase remain constant as all samples were optimum-cured. In the system, there will be physical and chemical crosslinks. The crosslinks formed during the vulcanization of NR and the polymerization of PS are purely chemical in nature and can be estimated

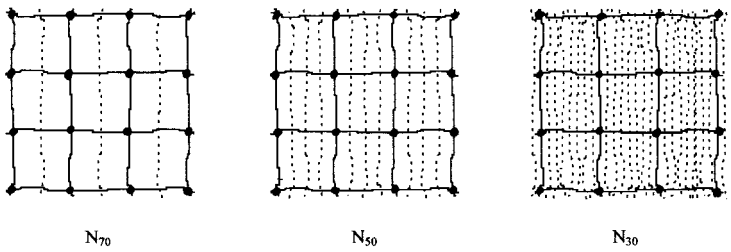

Figure 3 Schematic representation showing entanglement density for N_{70}, N_{50}, and N_{30} samples.

by the swelling method. In addition to this, physical crosslinks will be present due to polymer chain entanglements. As the PS content increases, the tendency to form chain entanglements increases. A schematic representation showing an entanglement density increase with the blend ratio is given in Figure 3. Therefore, as the PS content increases from 30 to 70, the number of polymer chains increases, resulting in increase in the semi-IPNs entanglement density, which, in turn, contributes to the increase in the crosslink density. In the S_3 series, the crosslink density values are comparatively high. This may be because DCP can introduce more strong chain interpenetration. The enhancement of properties in the S_3 series can be attributed to these higher crosslink density values. This is suggestive of a more compact and homogeneous morphology observed for the S_3 series, especially for S_3N_{30}.

Phase Morphology

The phase morphology was studied using a scanning electron microscope. Figure 4 shows a scanning electron micrograph of semi-IPNs. The morphology of 30 : 70, 50 : 50, and 70 : 30, NR/PS, DCP-initiated semi-IPNs (series 3) are shown in Figure 4(a–c), respectively. In all compositions, a distinct phase separation is not observed. A compact and homogeneous morphology was observed in all cases. In the S_1 series also, the same trend was observed. It is noticable that the N_{50} samples showed more phase separation than did the N_{30} and N_{70} samples. It is important to note that the NR phase which is crosslinked is continuous in all cases. In the N_{70} samples, as the PS content is low, PS forms the dispersed phase. Above 50% of PS, the PS phase also tends to be continuous. Therefore, a cocontinuous morphology was observed above 50% of PS. In Figure 5, the N_{50} samples of the S_1, S_2, S_3, and S_4 series are compared. The crosslink density values indicate that the highest extent of crosslinking and interpenetration occur in the S3 series. In all cases, phase separation was limited. The phase separation was least in the S_3N_{50} sample. The superior properties of the S_3 series may be due to this homogeneous phase morphology. In Figure 6, a schematic rep-

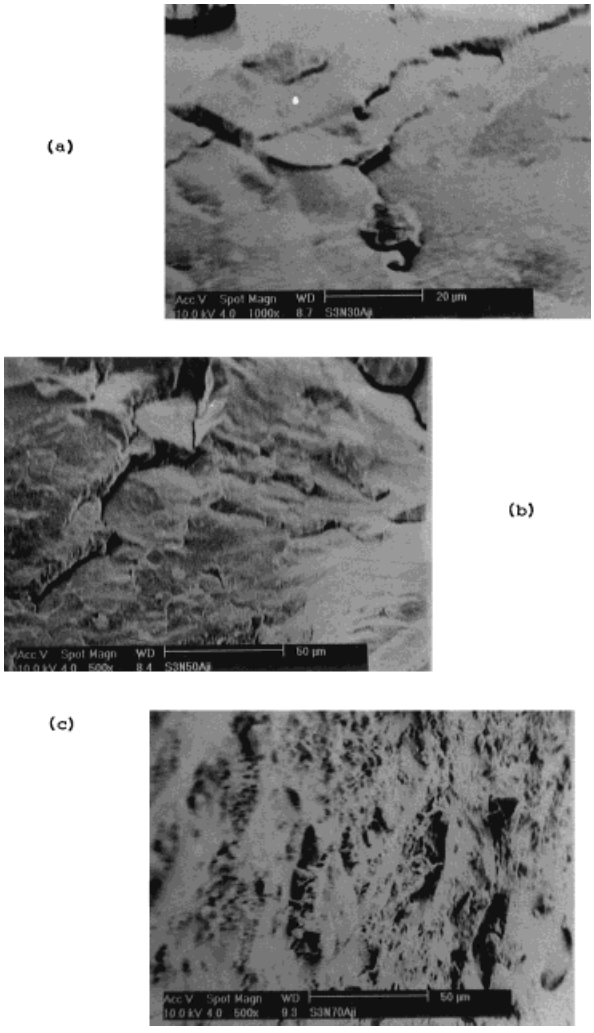

Figure 4 Scanning electron micrographs showing the effect of blend ratio on morphology: (a) S_3N_{30}; (b) S_3N_{50}; (c) S_3N_{70}.

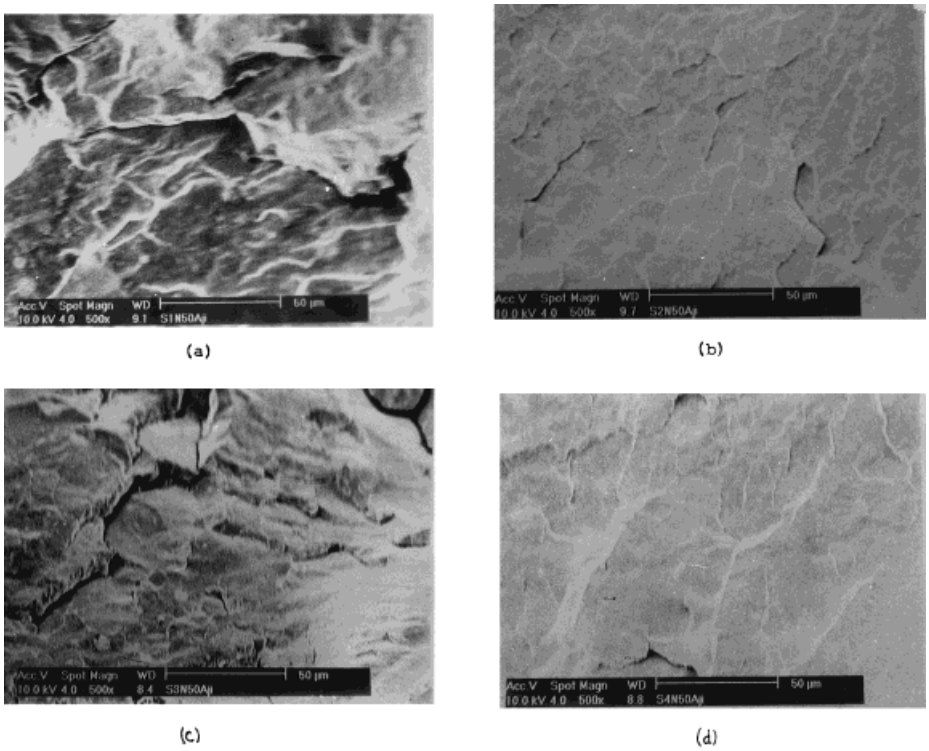

Figure 5 Scanning electron micrographs showing the effect of initiating systems on morphology: (a) S_1N_{50}; (b) S_2N_{50}; (c) S_3N_{50}; (d) S_4N_{50}.

resentation of the morphology of IPNs having different blend ratios are given. As the amount of PS increases, the size of the domain increases and finally becomes a continuous phase. Similar morphology representations were given by researchers earlier to give insight into the morphology and resultant properties of IPNs.[36]

Physical and Mechanical Properties

The variation of the semi-IPN sample density with the blend ratio was determined. The density values are given in Table IV. In all cases, the density increased with the PS content. Figure 7 shows the density of four sets of semi-IPNs at different blend ratios. The calculated density values are given by the dotted line. In all cases, the experimental value is above the theoretical value. This may be because the semi-IPN formed is a miscible system. This miscibility is induced due to high interpenetration. For miscible systems, the experimental value is usually higher than is the calculated one.[37,38]

The stress–strain curves for series 1 and 3 are shown in Figures 8 and 9, respectively. The deformation characteristics of each blend under an applied load is clear from the figures. As we go from 30 to 70 wt % of PS, the stress–strain curves show a gradual change from a rubbery to a plastic nature. The NR/PS 30 : 70 semi-IPN shows the typical plastic nature and the NR/PS 70 : 30 semi-IPN shows a rubbery nature. For samples where the PS content is above 50%, a yield point was observed. The deformation behavior of NR is typical of elastomers. On the addition of PS, the deformation pattern changes. When the PS content goes above 50%, the stress–strain curves show distinct elastic and inelastic regions. In the elastic region, yielding was observed. On increasing the PS in the blend content, the rubbery nature decreases and a necking tendency characteristic of plastics appears. Pure PS shows a brittle-type behavior.

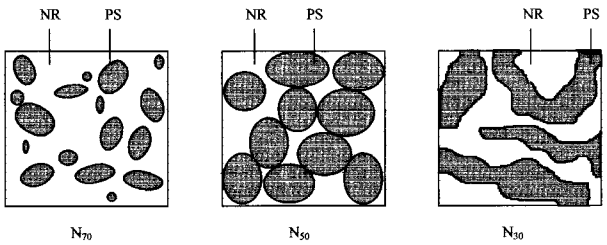

Figure 6 Schematic representation of morphology of IPNs: (a) N_{70}; (b) N_{50}; (c) N_{30}.

Table IV Effect of Composition on Mechanical Properties

Composition	Density (g/cc)	TS (MPa)	EB (%)	Tension Set (%)	Tensile Set (%)	Modulus at 50% Elongation (MPa)	Young's Modulus (MPa)
N_{100}	0.980	4.69	735	0	0	0.87	0.47
S_1N_{70}	1.061	5.40	642	10	10	1.80	8.50
S_1N_{50}	1.083	8.86	478	15	80	3.11	72.00
S_1N_{30}	1.090	11.85	352	105	130	12.86	145.20
S_2N_{70}	1.026	8.17	604	5	10	2.08	2.70
S_2N_{50}	1.076	11.19	561	50	80	5.57	3.22
S_2N_{40}	1.083	14.99	193	85	120	10.20	71.00
S_3N_{70}	1.063	5.69	585	10	10	1.18	1.70
S_3N_{50}	1.073	16.59	378	60	110	15.05	67.00
S_3N_{30}	1.078	25.01	260	125	140	42.97	371.60
S_4N_{70}	1.047	4.72	665	0	0	2.48	6.26
S_4N_{50}	1.062	11.18	534	10	35	5.22	27.00
S_4N_{30}	1.083	13.81	346	65	105	14.65	105.00
N_0	1.045	11.00	3	0	0	—	103.40

The Young's modulus of the semi-IPNs were determined from the stress–strain curves and the values are given in Table IV. In all four series, the values increase with increasing PS content. The modulus at 50% elongation was also determined from the stress–strain curves. The modulus values are given in Table IV. Above 50% of PS, a rapid increase in the modulus was observed. This indicates that the rubber phase was reinforced by the addition of the plastic phase. The system exhibits a high value of the modulus, especially the N_{30} samples. The modulus is the measure of the strength of the material. Therefore, it can be concluded that these IPNs exhibit good mechanical

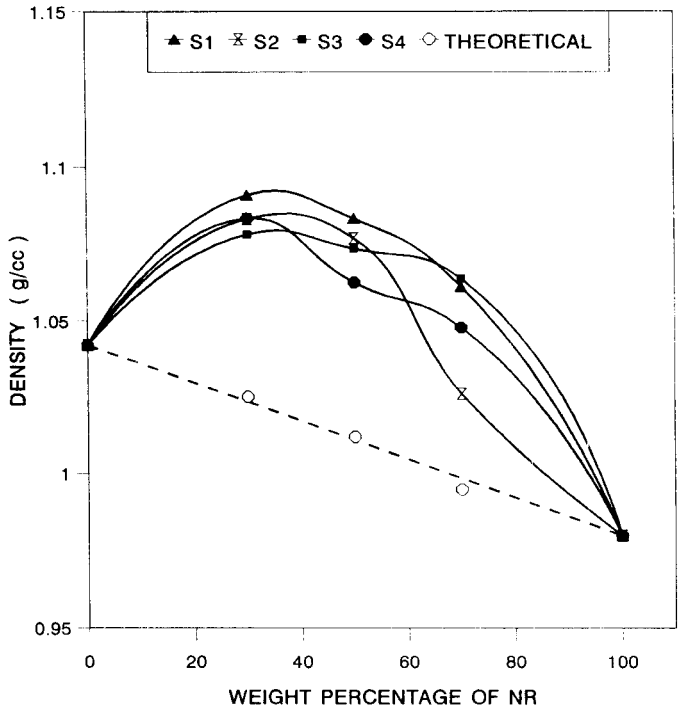

Figure 7 Density versus percentage of NR.

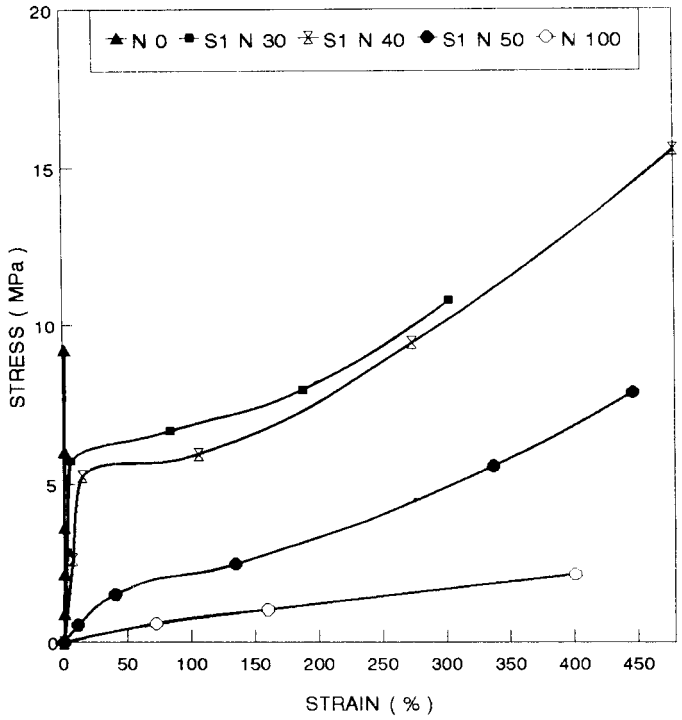

Figure 8 Stress–strain curves for series 1 (BPO).

properties. At 30% PS, the plastic phase reinforces the system, while at 30% of NR, the impact strength of PS is continuously enhanced. As a result, the material becomes tough and strong. Also from the morphology studies, it could be seen that at 30% PS (N_{30}) a highly compact and tight

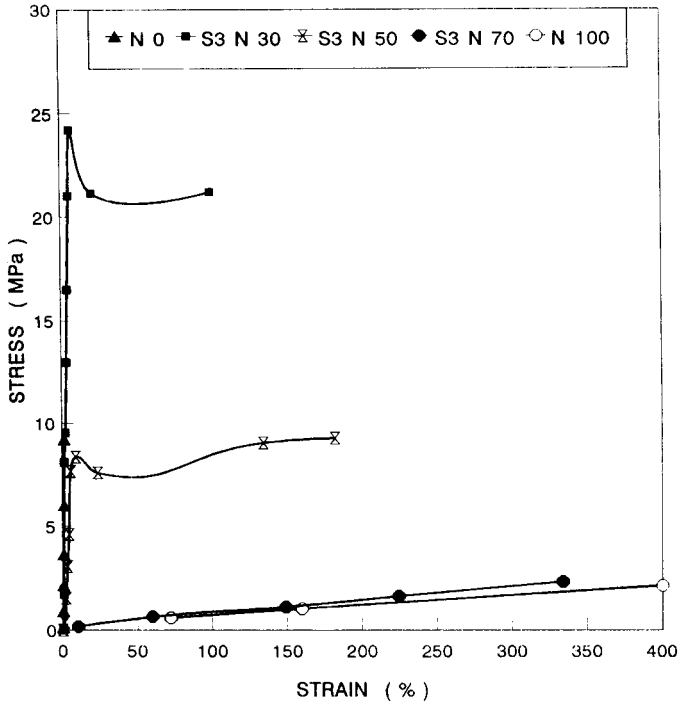

Figure 9 Stress–strain curves for series 3 (DCP).

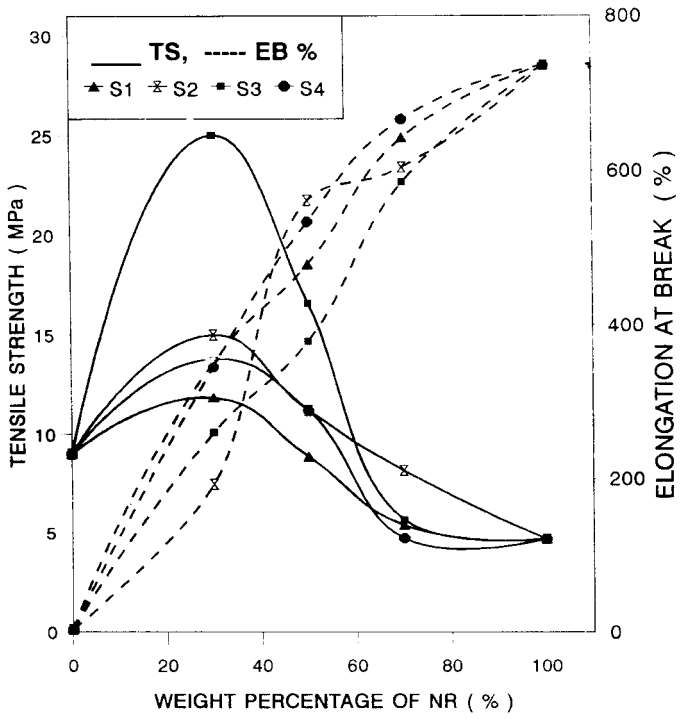

Figure 10 TS versus composition EB % versus composition.

polymer entanglement is developed which leads to superior properties.

The TS and elongation at break (EB %) of different semi-IPNs with different NR/PS compositons are given in Table IV. In all cases, the TS values were found to increase on the addition of PS to NR. It is also important to notice that the values were the highest in the case of DCP-initiated systems.

When we look at the EB % values, it was found that EB % decreases with decrease in the rubber content. The N_{70} semi-IPN has a high EB % while having low TS. The N_{30} IPN has low EB % with high TS. The N_{50} compositon showed a balancing of elongation at break and TS. Here, also, it is seen that the TS and EB % values were higher in the DCP-initiated series. Figure 10 shows the effect of the composition on the TS and elongation at break of the composites. The trend observed can be explained based on the crosslink density and phase morphology of the samples. The crosslink density increased as we moved from N_{70} to N_{30} samples. The crosslinks impart strength to the semi-IPN. As the crosslink density increases, the TS also increases. At the same time, elongation is restricted due to crosslinking. So, the EB % values decrease with the crosslink density. In the N_{30}, N_{50}, and N_{70} samples, it was found that the homogeneity was increased from N_{70} to N_{30}. The properties at each composition were dependent on the predominant phase. The N_{70} samples with greater NR content show a lower TS and high EB %. In the N_{50} samples, a balance of TS and EB % were observed. In the N_{30} samples, where PS is more compact and continuous, high TS and low EB % were observed. The formation of a compact and distinct phase distribution for high proportions of PS results in higher values of TS, tear strength, impact strength, and modulus. The low EB % was due to low elongation and brittleness of the PS phase. However, as the PS phase was not crosslinked, there was no drastic decrease in elongation.

The tension-set and tensile-set values of the semi-IPNs are given Table IV. The values increased with increasing PS content. The change in tensile set and tension set with IPN composition is shown. The IPN looses its rubbery nature or elasticity as the PS content increases. Therefore, the set increases. Also, in semi-IPNS with above 50% PS content, local plastic deformation was observed on the application of strain, while in the NR-rich system, elastic deformation of the rubber matrix was observed.

The tear load–displacement curves for series I and series III are shown in Figures 11 and 12, respectively. The neat NR samples show the larg-

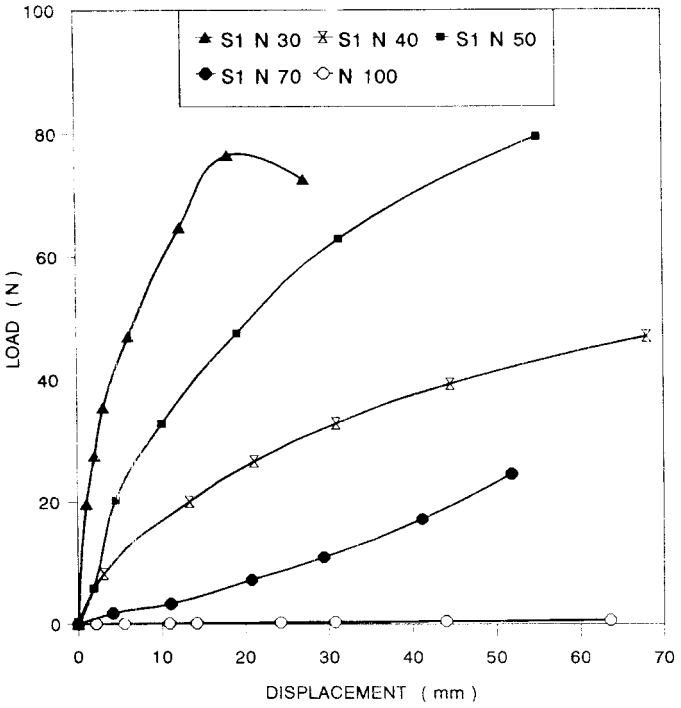

Figure 11 Load versus displacement curves for series 1.

est displacement with the minimum tearing force. On the addition of PS, the displacement decreases and the tearing load increases. The load is highest for the N_{30} samples.

The tear-strength values of all the IPNs were determined for the four series. The values are given in Table V. It was found that the tear-strength values increased with increase of the PS

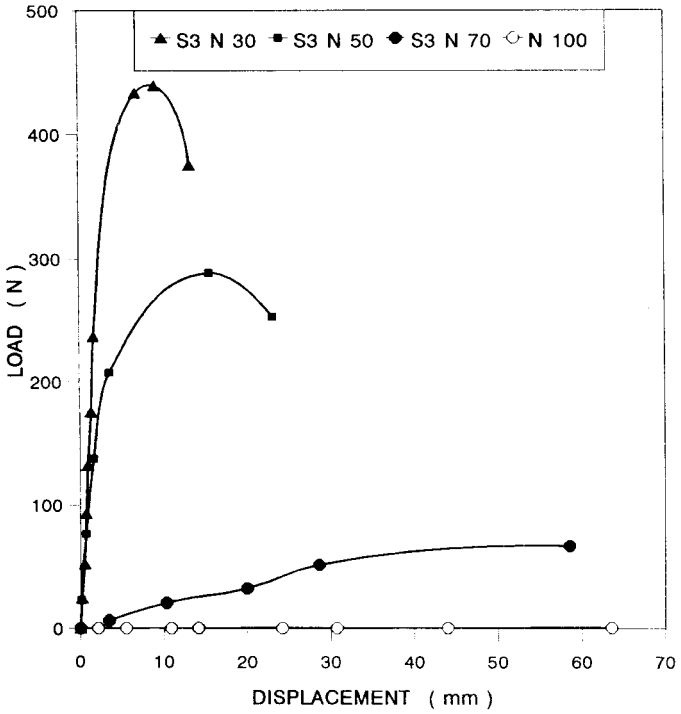

Figure 12 Load versus displacement curves for series 3.

Table V Effect of Blend Ratio and Initiating System on Hardness, Impact Strength, and Tear Strength

Sample Code	Tear Strength (N/m)	Impact Strength (N/m)	Hardness (Shore A)
N_0	—	56	97
S_1N_{30}	38.68	212	94
S_1N_{40}	—	200	—
S_1N_{50}	31.69	90	76
S_1N_{70}	17.54	[a]	72
S_2N_{40}	75.56	150	80
S_2N_{50}	44.98	94	73
S_2N_{70}	32.75	[a]	70
S_3N_{30}	146.90	102	91
S_3N_{40}	—	105	—
S_3N_{50}	87.16	167	75
S_3N_{70}	40.16	[a]	40
S_4N_{30}	62.43	225	85
S_4N_{40}	—	140	—
S_4N_{50}	37.25	107	76
S_4N_{70}	33.36	[a]	40
N_{100}	9.52	45	—

[a] Cannot determine the impact strength as the samples are flexible and rubbery.

content in each series. The tear-strength values are highest in the DCP series at all blend ratios. This can be explained based on the crosslink density. As the strength of the material is directly dependent on the crosslinking density, the tear-strength values vary directly with increasing crosslinking density.

The results of impact testings are given in Table V. The impact-strength results are found to exhibit an interesting trend: The N_{30}, N_{40}, and N_{50} samples (all the four series) showed good impact properties. The N_{70} samples are rubbery and flexible. So, the impact properties could not be determined. However, the property decreased in the order $N_{30} > N_{40} > N_{50}$ except for the DCP series. The N_{40} composition shows high values of impact. In the DCP series, the N_{50} samples showed the maximum impact strength. In the DCP system, the crosslink density makes the sample highly brittle at the N_{30} composition, making it less impact-resistant. The N_{30} sample can be considered as a rubber-toughened plastic. The rubber particles restrict the crack propagation. In the N_{30} sample, however, as the PS content is high, the IPN formed has some brittleness, which gives rise to a brittle failure. The mechanism changes from a brittle to a ductile fracture with increasing NR content. The fracture surface is more irregular in the N_{50} samples. It may be concluded that the NR phase is continuous in all compositions. Above 50% of PS, the PS phase also tends to be continuous, thus resulting in a cocontinuous system. This may be the reason for the marked enhancement of mechanical properties above 50% of PS. The hardness values are shown in Table V. It was found that the Shore A values increased with increasing PS content, as expected.

The increase in TS, tear strength, modulus, etc., can be considered as the reinforcement of the base material. By the addition of PS to NR, the mechanical strength of NR was enhanced and at the same time the brittleness of PS was reduced. Also, the modulus increased with increase in the PS content. The TS, tear strength, modulus, and set of the IPNs increased with increasing PS content, while elongation at break decreased with increasing PS content. As the PS content increases, the morphology becomes continuous and compact due to increase in the chain entanglements. This will also add to the enhancement of the mechanical properties.

Model Fitting

Various composite models such as the parallel model, the series model, the Halpin–Tsai equation, Coran's equation, and the Takayanaki model were made use of to study the mechanical behavior of the semi-IPNs. The parallel model (highest upper-bound model) is given by the equation[39]

$$M = M_1\phi_1 + M_2\phi_2 \tag{5}$$

where M is the mechanical property of the semi-IPN and M_1 and M_2 are the mechanical properties of the components 1 and 2, respectively, and ϕ_1 and ϕ_2 are the volume fractions of the components 1 and 2, respectively. In this model, the components are considered to be arranged parallel to one another so that the applied stress elongates each of the components by the same amount.

In the lowest lower-bound series model, the components are arranged in series with the applied stress. The equation is[40]

$$1/M = \phi_1/M_1 + \phi_2/M_2 \tag{6}$$

According to the Halpin–Tsai equation,[41,42]

$$M_1/M = (1 + AiBi\phi_2)/(1 - Bi\phi_2) \quad (7)$$

$$Bi = (M_1/M_2 - 1)/(M_1/M_2 + Ai) \quad (8)$$

In this equation, subscripts 1 and 2 refer to the continuous phase and the dispersed phase, respectively. The constant Ai is defined by the morphology of the system. For the hard domain dispersed in an elastomeric matrix, $Ai = 1.5$.

In the Coran model, the mechanical properties are generally in between the parallel model upper bound (M_U) and the series model lower bound (M_L). According to Coran's equation,[43]

$$M = f(M_U - M_L) + M_L \quad (9)$$

where f can vary between zero and unity. The value of f is a function of phase morphology and is given by

$$f = V_H n(nV_S + 1) \quad (10)$$

where n contains the aspects of phase morphology. V_H and V_S are the volume fractions of the hard phase and the soft phase, respectively.

In the Takayanaki model,[44–46]

$$M = (1 - \lambda)M_1 + \lambda[((1 - \phi)/M_1) + (\phi/M_2)] - 1 \quad (11)$$

where M_1 is the property of the matrix phase; M_2, the property of the dispersed phase; and ϕ, the volume fraction of the dispersed phase and is related to the degree of series–parallel coupling.

According to Cohen and Ramos,[47] the degree of parallel coupling of the model can be expressed by

$$\%\ \text{parallel} = [\phi(1 - \lambda)/(1 - \phi\lambda)] \times 100 \quad (12)$$

Kunori and Geil[48] suggested a model indicating that when a strong adhesive force exists between the blend components the dispersed phase will contribute to the strength of the blend. The equation is

$$\sigma_b = \sigma_m(1 - A_d) + \sigma_d A_d \quad (13)$$

Considering two possible fracture paths in a blend, eq. (13) can be modified as follows depending on whether the fracture is through the interface or through the matrix: When the fracture is through the interface,

$$\sigma_b = \sigma_m(1 - \phi_d^{2/3}) + \sigma_d\phi_d^{2/3} \quad (14)$$

and when the fracture is through the matrix,

$$\sigma_b = \sigma_m(1 - \phi_d) + \sigma_d\phi_d \quad (15)$$

where σ_b, σ_m, and σ_d are the properties of the blend, matrix phase, and dispersed phase, respectively, and ϕ_d, the volume fraction of the dispersed phase.

The Kerner equation[49,50] for perfect adhesion is given by

$$E = Ec\,\frac{\phi_d E_d/(7 - 5\nu_c)E_c + (8 - 10\nu_c)E_d + \phi_m/15(1 - \nu_c)}{\phi_d E_c/(7 - 5\nu_c)E_c + (8 - 10\nu_c)E_d + \phi_m/15(1 - \nu_c)} \quad (16)$$

where E, E_c, and E_d are the respective properties of the blend, continuous phase, and dispersed phase; ϕ_d and ϕ_m, the volume fractions of the dispersed and continuous phases; and ν_c, Poisson's ratio of the continuous phase. The values for ν_c are taken as 0.5 as the continuous phase is NR.

Figures 13 and 14 show the theoretical and experimental curves of the TS and Young's modulus values, respectively, for the four series. The theoretical curve based on eq. (14) comes closest to the experimental curve compared to other models. So, it may be concluded that the fracture path is through the interface rather than through the matrix. In the case of the Young's modulus (Fig. 14), the S_1 series having the lowest values fits with the Takayanaki model above 50% of PS and with the series model below 50% of PS.

For the tensile curves, it was found that the experimental values are above the theoretical values in all cases. The deviation of experimental values from theoretical values is more pronounced above 50% of PS. This may be because both the PS and NR phases have a cocontinuous morphology above 50% PS, rather than having a matrix-dispersed phase morphology.

Fractography

Fractography gives information about the mechanism of failure, type of load which caused the failure, and environmental effects which lead to failure. It is a fact that it is difficult to obtain the exact morphology of the fracture surface at the time of rupture, as there is a large deformation of polymers at the time of failure. There are gener-

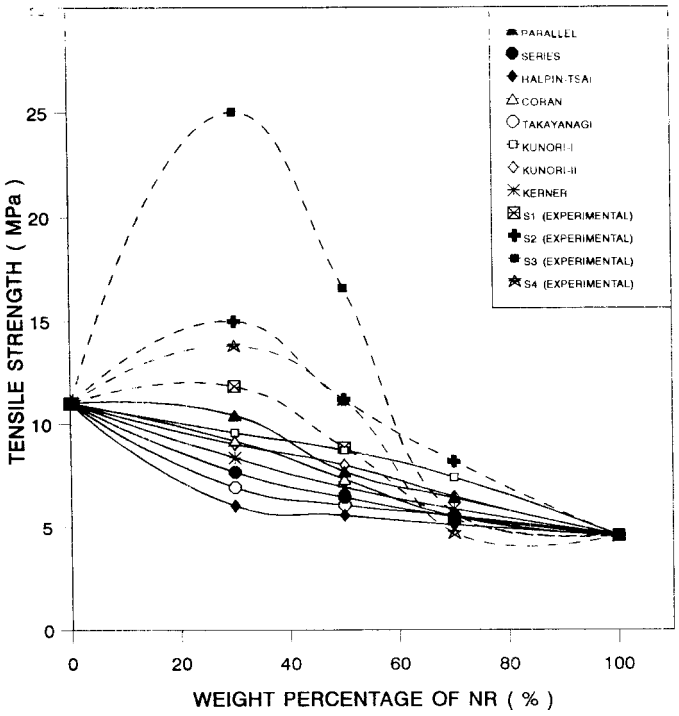

Figure 13 Model fitting (TS).

ally five modes of failure in macromolecular materials:

(a) Brittle failure where a crack is formed and propagated quickly with virtually no plastic deformation prior to failure.
(b) Ductile failure where plastic deformation and voids are produced in the material. The voids join together and failure occurs.
(c) In failure accompanied with crazing, voids are produced initiated from microirregularities. The voids are produced because of the movement of the surrounding molecular chains and crazing grows with orientation. The craze gradually changes into a crack and failure occurs.
(d) In boundary failure, failure occurs preferentially at the weakly bonded parts in the polymer sample.
(e) Fatigue failure is due to repeated application of stress relatively small compared to the TS of the material. The cracks produced due to repeated application of the stress join gradually with the principal crack and failure occurs.

The mode of failure can be studied in detail from the close observation of the fracture surfaces. The strength and properties of the samples can be explained based on the failure mode and nature of the fracture surface.

It was found that the N_{30} sample undergoes impact failure, giving rise to a regular pattern of the fracture surface. But in the N_{40} and N_{50} samples, regular path patterns were observed on the fracture surface. In the N_{40} sample, the failure may be by crazing. Multiple crazes are formed and this results in the high impact strength, even though PS content is lower than in N_{30}.

In NR/PS IPNs as PS content increases, the brittleness, the roughness of the fracture surface, and the strength increase, which is observed during mechanical testings. The tensile fracture surfaces are shown in Figure 15. It can be seen from 15(a) that in the N_{70} samples the fracture surface is smooth. In the S_1N_{70} sample [15(a)], the failure is by ductile fracture. In this case, large plastic deformation is observed. The cleavage occurs at the fracture surface as a result of step deformation and a partial ductile fracture produced by the intersection of slip planes. The high elongation at break is due to high NR content. The crosslinking allows the rubber to reach high strain by fibrillation. High strain and low stress at break were observed.

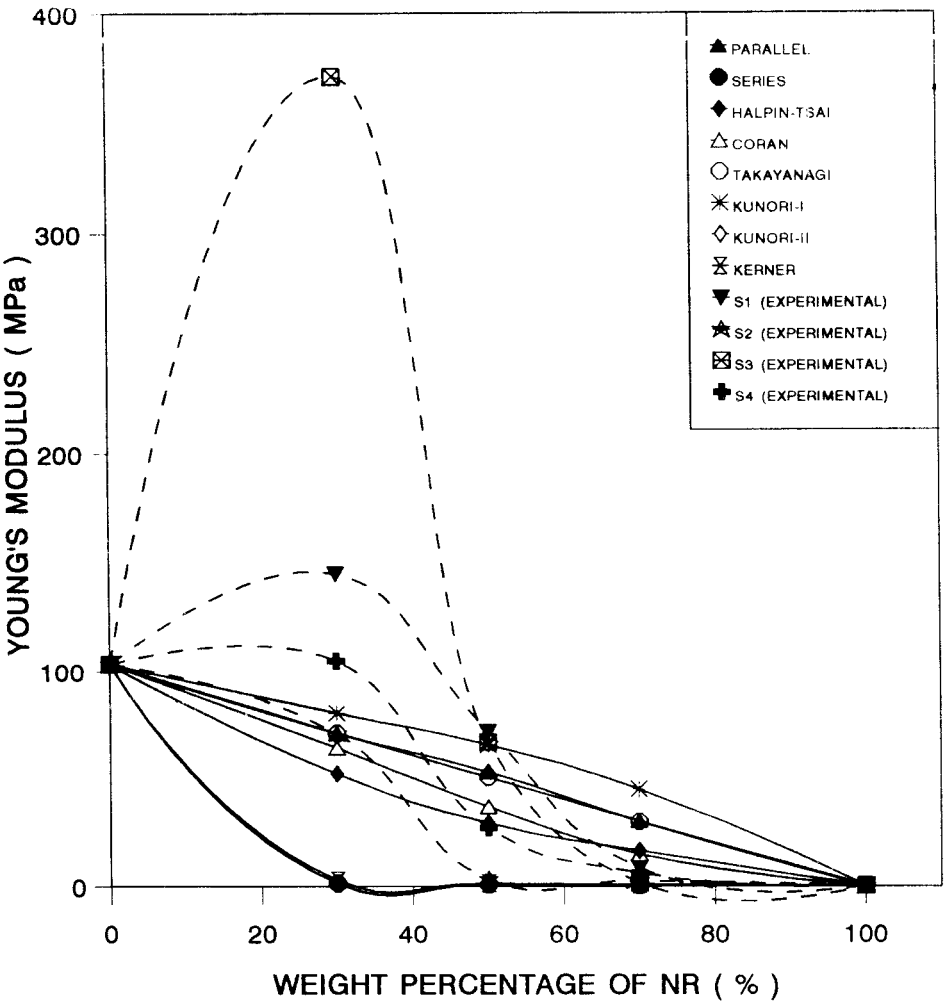

Figure 14 Model fitting (Young's modulus).

In the S_1N_{50} samples, the PS content is increased to 50% [Fig. 15(b)]. In this case, stress whitening is observed. Ribbonlike orientation bands which appear as a whitening phenomenon are observed in the direction of stress. The ribbonlike crazes are produced from voids. In the S_1N_{30} samples, the plastics phases increased to 70%. As PS content increases, the roughness of the fracture surface increases. The roughness is casued by primary cracks and secondary cracks and the roughness is high in brittle samples. A great degree of roughness is an indication of a low hysteresis loss of material. This was suggested earlier by Fukahori.[51] Stress whitening was observed as a result of multiple crack formation. As the NR content is low, it undergoes limited elongation. In this sample, at higher PS content, failure is by shear yielding and local plastic deformation, and stress whitening was observed. In the N_{50} samples, morphology is suggestive of shearing and drawing of the matrices.

When we look at the micrograph, it can be seen that in the N_{70} samples a simple crack or voiding is found on the fracture surfaces. In the N_{50} samples, the crack is irregular and some stress whitening is observed. In the N_{30} samples, a highly irregular fracture surface with a large number of microcracks (shear bands) was found. Microcrack formation helps in withstanding high energies. Microcracking (irregular fracture surface) increases with increase in PS content and a corresponding increase in TS is also observed.

The micrographs of the torn surfaces are shown in Figure 16. The effect of the blend ratio is clear from the SEM photograph. The N_{30}, N_{50}, and N_{70} semi-IPNs of the DCP-initiated system show tear surfaces with the sinusoidal structure along wavy crests and troughs. The wavy tear

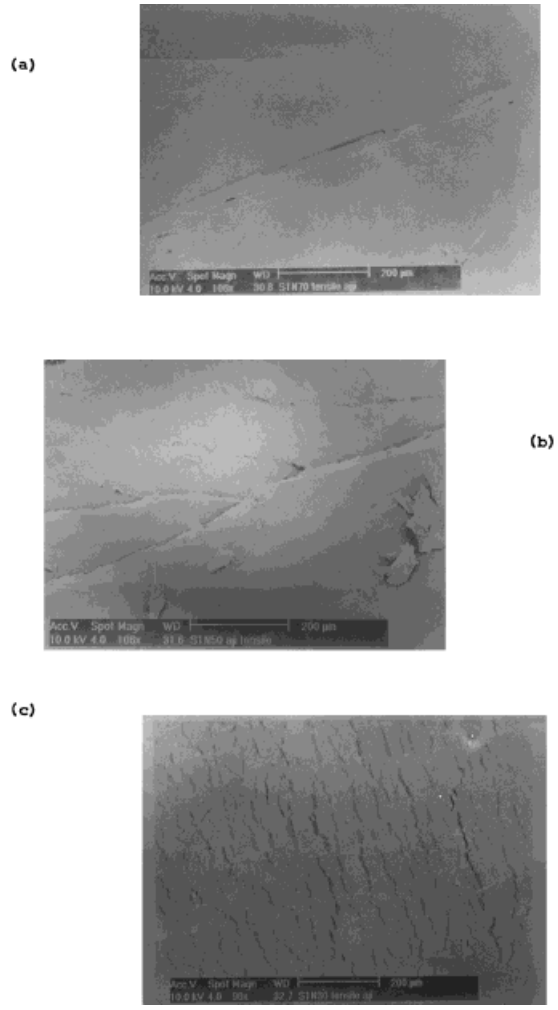

Figure 15 Scanning electron micrographs showing the tensile fracture surfaces of series 3: (a) S_1N_{70}; (b) S_1N_{50}; (c) S_1N_{30}.

fronts exhibit growing characteristics of a sine wave. The material which develops this structure is generally capable of withstanding high tearing forces. These patterns arise due to extensive stretching of the matrix along the stress direction to yield large plastic deformation. The wavy patterns were oriented in the system in the direction of the tearing force. The structure is most prominent in the N_{30} system which has the highest tear-strength values. The tear-strength values of semi-IPNs are also relatively high, supporting the development of a sinusoidal structure. In the S_3N_{70} sample, the foldings are less intense and the distance between two adjacent crests or troughs is 36.36 μm. In the S_3N_{50} samples, the foldings are more regular and distinct. The distance between two adjacent foldings is 45.45 μm. In the S_3N_{30} samples, the wavy foldings are highly prominant and closely packed, with an average distance of 113.6 μm between adjacent crests or troughs. The foldings on the fracture surface are generally intense and prominent for strong materials. So, it is clear that the S_3N_{30} samples show the highest tear strength. Similar observations were reported in other polymer blend systems which are characteristics of good tear-resistant materials.[52–54] Gent and Pulford correlated the tear strength of a polymer with the fracture surface morphology.[55] They measured the step spacing on the fracture surface and concluded that strong materials show closely spaced steps while weak materials show smooth torn surfaces. Some fine fibrous structures observed in the N_{30} sample are due to intrinsic crazes. These

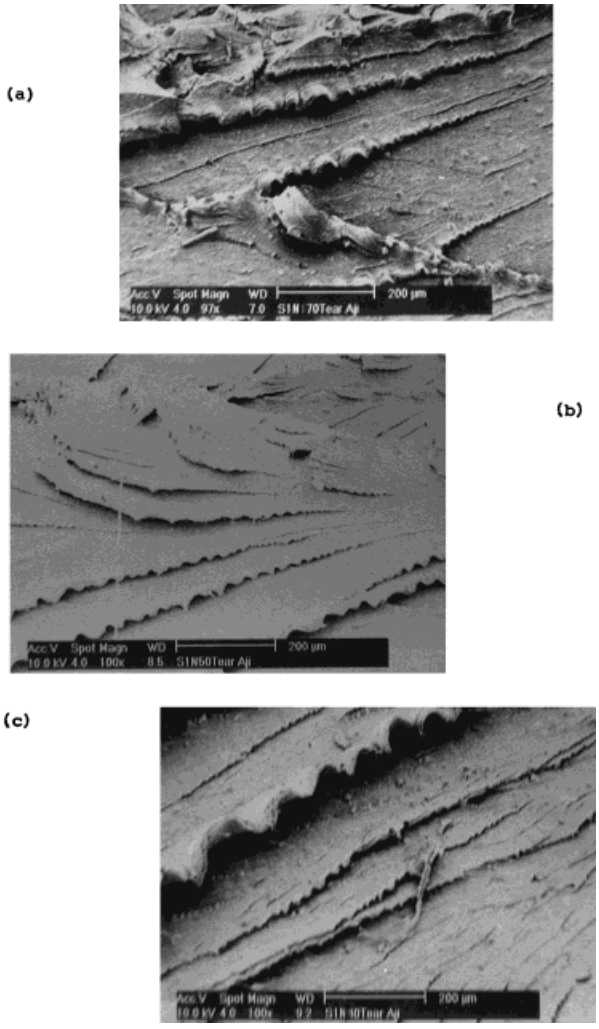

Figure 16 Scanning electron micrographs showing the tear surfaces: (a) S_3N_{70}; (b) S_3N_{50}; (c) S_3N_{30}.

intrinsic crazes are capable of withstanding high loads. This also helps the N_{30} samples to have a good tear-strength value.

CONCLUSIONS

A new class of semi-IPN polymers was developed from NR and the styrene monomer by the sequential method. In this method of synthesis, the crosslinked NR phase was prepared first. The linear PS phase was introduced into the crosslinked NR network by *in situ* polymerization. The IPN synthesis helps to have a better control on the morphology and intimate mixing of the two component phases. As a result of this type of preparation, a finer and more uniform distribution of PS in the NR phase is obtained.

The morphology studies using SEM revealed a compact and homogeneous morphology for the IPNs developed. The IPNs have a very ordered and compact arrangement of the two phases. Microlevel mixing of the components is possible in this method by introducing homogeneity in the IPN developed. The superior properties of IPNs is due to the intimate intermixing of the phases. The SEM micrographs showing the morphology also reveals a homogeneous dispersion of the two phases. The variation of the properties of different semi-IPNs is dependent on the blend ratio and the nature of initiating system for styrene. The properties of the major component is predominant in the resultant IPN. In 50 : 50 semi-IPNs, a balance of properties is observed.

It is found that in all cases as the PS content increases the TS, tear strength, modulus, impact strength and hardness, and tensile set and tension set increase. The EB % values decrease due to decrease in the elasticity of the material with a decreasing NR content. The tensile fracture surface showed a failure mechanism changing from elastic failure to local plastic deformation as the PS phase increases. The entanglement density also increases with increasing PS content, thus explaining the improvement in the mechanical properties with the PS content. It is also concluded that the system shows a cocontinuous morphology above 50% PS. This results in the enhancement of properties above 50% of PS.

The experimental values are fitted into various models and it was found that the fracture is through the interface between the matrix and dispersed phase. It is also found that the values deviate from the theoretical ones above 50% of PS content, supporting the fact that above 50% of PS a cocontinuous morphology is developed.

One of the authors (A. P. M.) is grateful to the Council of Scientific and Industrial Research, New Delhi, for a Senior Research Fellowship (SRF). The authors are thankful to the Third World Academy of Sciences (TWAS, Italy) for financial support.

REFERENCES

1. Hsieh, K. H.; Hung, W. Y.; Liao, D. C.; Kao, S. C. J Appl Polym Sci 1993, 57, 319.
2. Chou, Y. C.; Lee, L. J Polym Eng Sci 1992, 35, 976.
3. Rennar, N.; Opermann, W. Colloid Polym Sci 1992, 270, 527.
4. Yenwo, G. M.; Manson, J. A.; Pulido, J.; Sperling, L. H.; Conde, A.; Devia, N. J Appl Polym Sci 1977, 21, 153.
5. Sionakidis, J.; Sperling, L. H.; Thomas, D. A. J Appl Polym Sci 1979, 24, 1179.
6. Xue, Y.; Frisch, H. L. J Polym Sci Chem 1993, 31, 2165.
7. Das, B.; Chakraborthy, D. Polym Gels Network 1995, 3, 197.
8. Das, B.; Sinha, S.; Gangopadhyay, T. Eur Polym J 1993, 29, 57.
9. Tung, C. J.; Hsu, T. C. J. J Appl Polym Sci 1992, 46, 1759.
10. Donatelli, A. A.; Sperling, L. H.; Thomas, D. A. Macromolecules 1976, 9, 676.
11. Klempner, D.; Frisch, K.; Frisch, H. L. J Elastoplast 1973, 5, 196.
12. Donatelli, A. A.; Sperling, L. H.; Thomas, D. A. Macromolecules 1976, 9, 671.
13. Das, B.; Gangopadhyay, T.; Sinha, S. J Appl Polym Sci 1994, 54, 367.
14. Das, B.; Gangopadhyay, T. Eur Polym J 1992, 28, 867.
15. Kelley, S. S.; Ward, T. C.; Wolfgang, C. J Appl Polym Sci 1990, 41, 2813.
16. Ruchenstein, E.; Li, H. J Appl Polym Sci 1995, 55, 961.
17. Frisch, H. L.; Xue, Y. Polym J 1994, 26, 828.
18. Sperling, L. H. IPN and Related Materials; Plenum: New York, 1981; Chapter 6.
19. Mai, K.; Zeng, H. J Appl Polym Sci 1994, 53, 1653.
20. Rajalingam, R. P.; Radhakrishnan, P.; Feromin, D. J. Met Meter Proc 1989, 1, 197.
21. Chern, Y. C.; Hsieh, K. H.; Ma, C. C. M.; Gong, Y. G. J Mater Sci 1994, 29, 5435.
22. Kim, S. C.; Klempner, D.; Frisch, K. C.; Frisch, H. L.; Ghiradella, H. Polym Eng Sci 1975, 15, 339.
23. De Graaf, L. A.; Beyer, J.; Moller, M. J Polym Sci Part B Polym Phys 1995, 3, 1073.
24. Verchere, D.; Pascault, J. P.; Sautercace, H.; Moschair, S. M.; Riccard, C. C.; William, R. J. J. J Appl Polym Sci 1991, 42, 701.

25. Jia, D.; Pang, Y.; Liang, X. J Polym Sci Part B Polym Phys 1994, 32, 817.
26. Yenwo, G. M.; Sperling, L. H.; Manson, J. A.; Conde, A. In Chemistry and Properties of Crosslinked Polymers; Labana, S. S., Ed.; Academic: New York, 1973.
27. Ramaraj, B.; Radhakrishnan, G. J Appl Polym Sci 1994, 52, 837.
28. May, C. A.; Tanaka, G. Y. Epoxy Resin Chemistry and Technology; Marcel Dekker: New York, 1973.
29. Epoxy Resin Chemistry; Advances in Chemistry 114; Bauer, R. S., Ed.; American Chemical Society: Washington, DC, 1979.
30. Mathew, A. P.; Packirisamy, S.; Kumaran, M. G.; Thomas, S. Polymer 1995, 36, 4935.
31. Mark, H. F.; Bikales, N. M.; Overberge, C. G.; Menges, G.; Eds. Encylopaedia of Polymer Science and Engineering; Wiley: 1986; Vol. 4, p 356.
32. George, S. C.; Ninan, K. N.; Thomas, S. Polym Int, in press.
33. Aminabhavi, T. M.; Phayde, H. T. S. Polymer 1995, 36, 1023.
34. Flory, P. J.; Rehner, J. J. J Chem Phys 1943, 11, 521.
35. Jain, S. R.; Sekkar, V.; Krishnamurthy, V. N. J Appl Polym Sci 1993, 48, 1515.
36. Hu, R.; Dimonic, V. L.; El-aasser, M. S.; Pearson, R. A.; Hiltner, A.; Mylonakis, S. G.; Sperling, L. H. J Polym Sci Part B Polym Phys 1997, 35, 1501.
37. Varughese, K. T.; Nando, G. B.; De, P. P.; De, S. K. J Mater Sci 1988, 23, 3894.
38. Korotneva, L. A. Eur Polym J 1976, 12, 817.
39. George, S.; Prasannakumari, L.; Koshy, P.; Varughese, K. T.; Thomas, S. Mater Lett 1996, 26, 51.
40. George, S.; Joseph, R.; Varughese, K. T.; Thomas, S. Polymer 1995, 36, 4405.
41. Nielson, N. E. Rheol Acta 1974, 13, 86.
42. George, S.; Prasannakumari, L.; Koshy, P.; Varughese, K. T.; Thomas, S. Mater Lett 1996, 26, 51.
43. Coran, A. Y. In Hand Book of Elastomers, New Development & Technology; Bhowmick, A. K.; Stephens, H. L., Eds.; Marcel Dekker: New York, 1988; p 249.
44. Takayanaki, M. Mem Fac Eng Kyushu Univ 1963, 23, 57; Proc IV Int Cong Rheol 1965, 161.
45. Holsti-Miettinen, R. M.; Seppala, J. V.; Ikkala, O. T.; Reima, I. T. Polym Eng Sci 1994, 34, 395.
46. Ramos, A. R.; Cohen, R. E. Polym Eng Sci 1977, 17, 639.
47. Cohen, R. E.; Ramos, A. R. J Macromol Sci Phys B 1980, 17, 625.
48. Kunori, T.; Geil, P. H. J Macromol Sci Phys B 1980, 18, 135.
49. Beahan, P.; Thomas, A.; Bevis, M. J Mater Sci 1976, 11, 1207.
50. Kerner, E. H. Proc Phys Soc Lond Sect 1956, 13, 69, 808.
51. Fukahori, Y. Nippon Gomu Kyokaishi 1982, 55, 82.
52. Varghese, H.; Bhagawan, S. S.; Prabhakaran, N.; Thomas, S. Mater Lett 1995, 24, 333.
53. Bhagawan, S. S.; Tripathy, D. K.; De, S. K. J Mater Sci 1987, 6, 157.
54. Varughese, K. T.; Nando, G. B.; De, S. K.; Sanyal, S. K. J Mater Sci 1989, 24, 3491.
55. Gent, A. N.; Pulford, C. T. R. J Mater Sci 1984, 19, 3612.